

# Growth activity during fingering in a porous Hele Shaw cell

Grunde Løvoll,<sup>1,2,3</sup> Yves Méheust,<sup>2,3,1</sup> Renaud Toussaint,<sup>1,2</sup> Jean Schmittbuhl,<sup>3</sup> and Knut Jørgen Måløy<sup>1</sup>

<sup>1</sup>*Department of Physics, University of Oslo, Norway*

<sup>2</sup>*Department of Physics, NTNU Trondheim, Norway*

<sup>3</sup>*Laboratoire de Géologie, École Normale Supérieure, Paris, France*

(Dated: July 12, 2021)

We present in this paper an experimental study of the invasion activity during unstable drainage in a 2D random porous medium, when the (wetting) displaced fluid has a high viscosity with respect to that of the (non-wetting) displacing fluid, and for a range of almost two decades in capillary numbers corresponding to the transition between capillary and viscous fingering. We show that the invasion process takes place in an active zone within a characteristic screening length  $\lambda$  from the tip of the most advanced finger. The invasion probability density is found to only depend on the distance  $z$  to the latter tip, and to be independent of the value for the capillary number  $C_a$ . The mass density along the flow direction is related analytically to the invasion probability density, and the scaling with respect to the capillary number is consistent with a power law. Other quantities characteristic of the displacement process, such as the speed of the most advanced finger tip or the characteristic finger width, are also consistent with power laws of the capillary number. The link between the growth probability and the pressure field is studied analytically and an expression for the pressure in the defending fluid along the cluster is derived. The measured pressure are then compared with the corresponding simulated pressure field using this expression for the boundary condition on the cluster.

PACS numbers: 47.20.Gv, 47.53.+n, 47.54.+r, 47.55.-t, 47.55.Mh, 68.05.-n, 68.05.Cf, 81.05.Rm.

## I. INTRODUCTION

Different types of unstable fluid displacements in porous media play an important role in many natural and commercial processes [1, 2]. Developments of a better understanding of these processes therefore has a broad scientific interest as well as potentially huge economical benefits. The complex patterns observed in such processes have been extensively studied and modeled over the last decades, see [1, 2, 3, 4, 5, 6, 7] and references therein.

The geometry of the displacement structures observed in immiscible two phase flow are in general controlled by the competition between viscous forces, gravitational forces, capillary forces; those various forces act on scales ranging from the pore scale to the system size. The relative wettabilities, viscosities, and densities of the fluids, as well as the heterogeneity of the underlying porous media, play an important role in the competition process. The relative magnitudes of viscous and capillary forces (on pore scale) are quantified through the dimensionless *capillary number*  $C_a = (\mu_w v_f a^2)/(\gamma \kappa)$  where  $\mu_w$  is the viscosity in the wetting (displaced) fluid,  $v_f$  is the filtration speed,  $a$  is the characteristic pore size,  $\gamma$  is the interface tension, and  $\kappa$  is the permeability of the porous medium.

In this paper we address a drainage experiment in which non-wetting air displaces a high viscous wetting glycerin/water solution in a horizontal two-dimensional porous medium; hence, gravity has no influence on the displacement. We investigate the crossover regime between the regime of slow displacement for which capillary forces control the dynamics of the invasion process and

the geometry of the resulting invasion structure (capillary fingering), and that of fast displacements where viscous forces are dominant (viscous fingering). We emphasize on the dependence of the invasion probability density  $\phi$ , or activity, on the distance to the most advanced finger tip along the interface. The invasion probability density  $\phi$  is the growth probability of the invasion structure; it is fundamental because both the structure and the dynamics are controlled by this function. Growth probability has been discussed extensively in the past for DLA (Diffusion Limited Aggregation) simulations [8, 9, 10, 11, 12, 13] where it was found to be a multifractal distribution or a harmonic measure [11, 12, 13, 14]. A strong analogy exists between the structures obtained by DLA and by viscous fingering in a porous medium, as was first pointed out by Paterson [15]. However, the dynamics of the two processes differ in that there is no surface tension for the DLA, in contrast to drainage in porous media where surface tension gives rise to capillary pressure thresholds at the pore scale. The capillary pressure threshold values, introduce a lower cut off for the invasion probabilities, even for fast flows. In the slow displacement limit for which  $v_f \simeq 0$ , the invasion process is entirely controlled by the fluctuations of the capillary threshold distribution inside the porous medium [6, 16].

Imbibition experiments (wetting fluid displacing a non wetting fluid) were previously performed in a quasi two-dimensional system [17, 18], where the width of the viscous fingers was measured to scale with the capillary number as [17, 18]  $w_f \propto C_a^{-0.5}$ . This scaling relation was explained by a strong dynamic component of the capillary pressure [18]. We do not observe a strong dynamic component of the capillary pressure in our experiments (see below). The geometry of the invader for drainage is

also significantly different from the invader structure of imbibition [17, 18, 19, 20].

In this study we study experimentally the growth probability density  $\phi(z)$  as a function of the distance  $z$  (in the flow direction) from the most advanced finger tip, and its dependence on the extraction speed (or capillary number). We also investigate experimentally the mass density  $n(z)$  along the flow direction of the invader, and confront the behavior of the measured  $\phi(z)$  and  $n(z)$  to what we expect from analytical arguments. A calculation of the  $z$  dependence of the pressure on the surface of the invader is presented, which yields the  $z$  dependence of the capillary pressure and shows a direct link with the measured growth probability density. Pressure measurements are performed in the model and compared with pressures simulated by solving the Laplace equation with this pressure boundary condition. Other features characteristic of the displacement, such as outermost tip velocity and the width of the invasion fingers, are also investigated.

The present article is organized as follows. We first present the experimental method (section II). We then discuss the experimental results (section III), before concluding (section IV).

## II. EXPERIMENTAL METHOD

The experimental setup is shown in Fig. 1. The porous model consists of a mono-layer of glass beads of diameter  $a = 1$  mm which is randomly spread between two contact papers [21, 22]. The model is a transparent rectangular box of dimensions  $L \cdot W$  and thickness  $a$ .

Two models of widths  $W = 430$  mm and  $W = 215$  mm have been used in the experiments; their other characteristics were identical. They are respectively referred to in the rest of the article as the “wide” and the “narrow” model.

To prevent bending of the model a 2 cm thick glass plate and a 2 cm thick Plexiglas plate are placed on top of the model. To squeeze the beads and the contact paper together with the upper plate, a mylar membrane mounted on a 2.5 cm thick Plexiglas plate, below the model, is kept under a 3.5 m water pressure as a “pressure cushion”. The upper and the lower plates are kept together by clamps, and the side boundaries are sealed by a rectangular silicon rubber packing. Milled inlet and outlet channels are made in the upper Plexiglas plate. The distance between the inlet and outlet channels define the length of the model  $L = 840$  mm. One should also note that a few beads are removed from a small region near the center of the inlet channel, to initiate the invader in the center of the inlet. This is done to avoid edge effects appearing when the invader grows to the lateral boundaries of the model. The porosity of the models is measured to be 0.63 and the permeability is  $\kappa = (0.0166 \pm 0.0017) \cdot 10^{-3} \text{ cm}^2 = (1685 \pm 175)$  Darcy.

The defending wetting fluid used in all our experi-

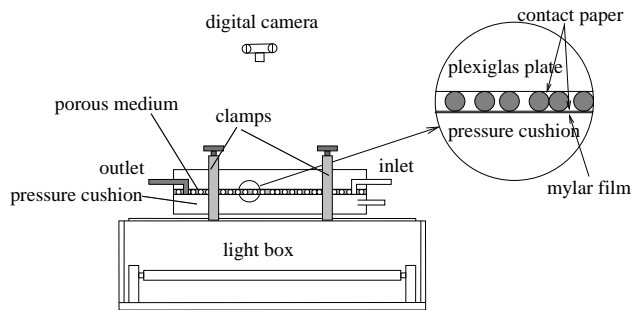


FIG. 1: Sketch of the experimental setup with the light box for illumination, the porous model and the digital camera. The porous medium is sandwiched between two contact papers and kept together with a “pressure cushion”.

ments is a 90% – 10% by weight *glycerol-water* solution dyed with 0.1% Negrosine to increase the contrast between the colored fluid and the invader. Air is used as the invading non-wetting fluid. The *wetting* glycerol-water solution has a viscosity of  $\mu_w \approx 0.165$  Pa.s and a density of  $\rho_w = 1235 \text{ kg.m}^{-3}$  at room temperature. The corresponding parameters for the *non-wetting* air are  $\mu_{nw} = 1.9 \cdot 10^{-5}$  Pa.s and  $\rho_{nw} = 116 \text{ kg.m}^{-3}$ . The viscous ratio is thus  $M = \mu_{nw}/\mu_w \sim 10^{-4}$ . The surface tension between these two liquids is  $\gamma = 6.4 \cdot 10^{-2} \text{ N.m}^{-1}$ . The temperature in the defending fluid is controlled and measured at the outlet of the model during each experiment, so as to accurately estimate the viscosity of the wetting fluid.

The absolute pressure in the wetting liquid is measured in the outlet channel and at a point at a distance of 280 mm (in the flow direction) from the inlet channel and 38 mm from the left boundary (looking in the flow direction) using *Honeywell 26PCAFlow-Through* pressure sensors.

The invader is visualized by illuminating the model from below with a light box and taken pictures with a *Kodak DCS 420 CCD* camera, which is controlled by a computer over a SCSI connection. This computer records both the pictures and the pressure measurements. Each image contain  $1536 \times 1024$  pixels, which corresponds to a spatial resolution of 0.55 mm per pixel or  $\sim 3.22$  pixels per pore ( $1 \text{ mm}^2$ ); the color scale contains 256 Gray levels. The Gray level distribution of the image presents two peaks corresponding respectively to the white air-filled and dark gray glycerol-filled parts of the image. The image is filtered so as to obtain a clear boundary between the two phases, through a scheme that mainly consists in removing the background and thresholding at a gray level value between the two latter peaks. All further image treatments are performed on the resulting black and white image.

To check possible dynamic components of the capillary pressure we performed gravity stabilized experiments by keeping the experimental model vertical [22] and extracting the glycerol/water mixture from the bottom of the

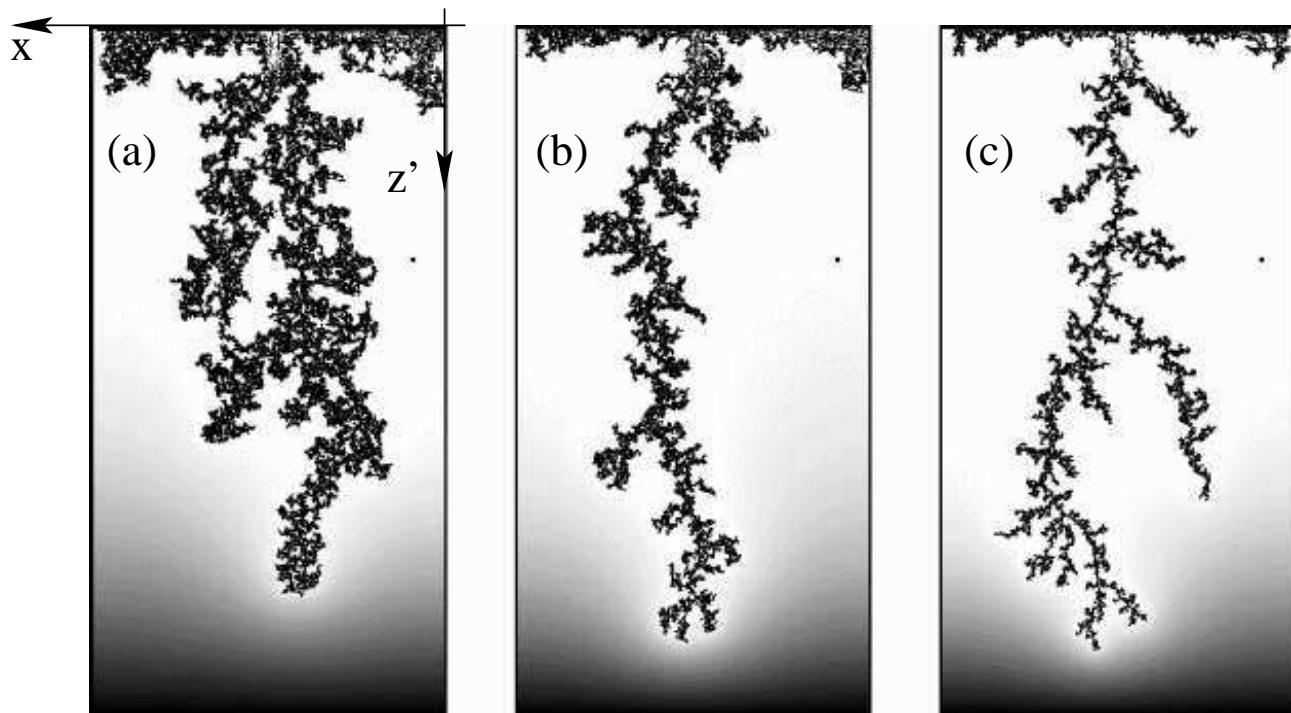


FIG. 2: Displacement structures obtained for different withdrawal rates: (a)  $C_a = 0.027$ , (b)  $C_a = 0.059$  and (c)  $C_a = 0.22$ . The images have been treated to separate the two phases, excluding the invasion structure close to the inlet. The black frame denotes the outer boundaries of the model, while the black spot close to the right edge of the model denotes the position of the pressure sensor. The simulated pressure field is shown superimposed on the image. Dark shadings correspond to low pressures while light shadings correspond to high pressures.

model. The capillary pressure was measured by recording the pressure in the model as the stabilized fluid front approaches the sensor. No systematic dynamic effect on the capillary pressure was found. For the low injection rates the width of the fronts was further used to estimate the minimum and width  $W_c$  of the capillary pressure threshold distribution.

Throughout the paper the following coordinate system is used:  $(x, z')$  is the orthonormal frame describing the porous medium plane, with  $z'$  the spatial coordinate in the direction of the flow (positive in flow direction). The position of the most advanced finger tip is denoted  $z'_{tip}$ ; its speed along the  $z'$  axis is denoted  $v_{tip} = \dot{z}'_{tip}$ . The position along the  $z'$  axis computed with respect to that of the most advanced finger tip is  $z = z'_{tip} - z'$ . Those coordinates are indicated in Fig. 2 and 3.

### III. RESULTS

We present 12 experiments using the wide model for values of the capillary number  $C_a$  ranging from  $1.4 \cdot 10^{-2}$  to  $3.6 \cdot 10^{-1}$  and 5 experiments using the narrow model, for capillary numbers ranging from  $3.3 \cdot 10^{-2}$  to  $1.9 \cdot 10^{-1}$ . The latter series was conducted to check system size dependencies. For every experiment, we have carefully investigated the invasion process.

Fig. 2 displays air clusters observed for the same porous medium, at three different flow rates. The “fingers” look visually thinner at increased invasion speed and more internal trapping of the defender is observed at low speed. Hence, the displacement exhibits obvious capillary number dependent features which will be discussed in details in part B below. In part A, we focus on the relation between the growth activity, the frozen structure left behind and the pressure field in front of the fingers.

#### A. The relation between growth activity, frozen structure and fluid pressures.

The growth activity has been investigated by measuring the growth probability density  $\phi(z)$  from series of images and performing pressure measurements.

##### 1. Definition of growth probability density $\phi(z)$ and mass density $n(z)$ .

To investigate the growth process, images have been taken with constant time  $\Delta t$  between each image. The tip position of the longest finger is identified to find the coordinate system  $(x, z)$ , and to be able to calculate the speed of the longest finger. The differential growth be-

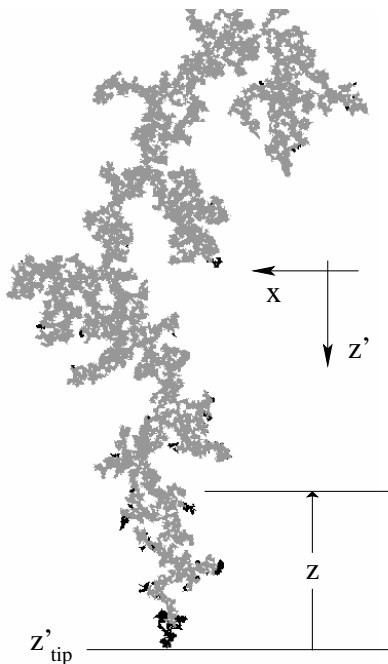


FIG. 3: Two consecutive images taken at a time interval  $\Delta t \simeq 15$  during the experiment at  $C_a = 0.059$ , drawn on top of each other. The invaded regions in the first image are painted light gray, the growth areas obtained by subtracting the first picture from the other one are painted black. The coordinate system used throughout the paper is also shown.

tween two images is found by a direct image subtraction between two subsequent images. After the subtraction we typically have a collection of invaded pores representing the growth (see Fig. 3). The growth density  $\phi^*(z)$  is defined as the average number of filled pores within  $[z, z + \Delta z]$  divided with  $\Delta z$ . After an initial regime corresponding to the time needed for the longest finger to propagate the order of the width of the porous medium  $W$ ,  $\phi^*(z)$  is found to be fairly independent of time up to a few percents variations. In a given experiment with constant  $C_a$ ,  $\phi^*(z)$  is then averaged over all images excluding this initial regime, to obtain a good average of the stationary growth function. The growth probability density  $\phi(z) = K \phi^*(z)$ , where  $K$  is a normalization constant, is then found by normalizing  $\phi^*(z)$  with respect to  $z$  such that

$$\int_0^L \phi(z) dz = 1. \quad (1)$$

Note that in the remainder of the paper  $z$  is in units of pore size ( $a = 1$  mm).

The mass density of the frozen structure  $n(z)$  is defined as the average number of filled pores within  $[z, z + \Delta z]$  divided with  $\Delta z$ . The average is taken over all images in a given experiment with constant  $C_a$ . Both  $n(z)$  and  $\phi(z)$  appeared to be fairly robust with respect to the width  $\Delta z$  of the analysis strips used to compute them.

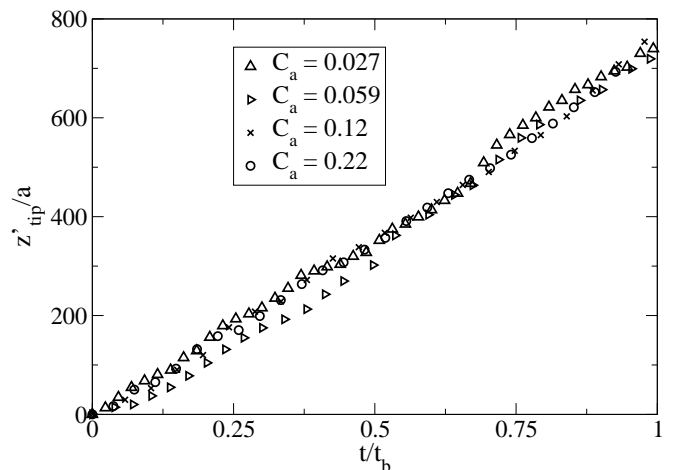


FIG. 4: Plot of the position of the most advanced finger tip  $z'_{tip}$  as a function of time. Data from the wide model. The time is rescaled by dividing with the break through time  $t_b$ , which is the time the most advanced fingers reach the outlet channel. The values of  $t_b$  are 5347 s, 1204 s, 476 s and 256 s for the capillary numbers  $C_a$  equal to 0.027, 0.059, 0.12 and 0.22 respectively.

## 2. Growth activity and the frozen structure left behind

For all experiments, the speed of the most advanced finger tip was observed to be fairly constant. Fig. 4 shows the position of the most advanced finger tip  $z'_{tip}$  for different capillary numbers. After a short initial stage, the speed of the fingers saturates to a constant average value. Linear fits to the behavior  $z'_{tip}$  as a function of time outside the initiation stage provide an average finger tip speed  $v_{tip}$  for all experiments.

The measured invasion probability density function  $\phi(z)$  is plotted in Fig. 5 as a function of the distance to the finger tip for the two system sizes on a lin-log plot. An exponential like decay is seen for  $z/a < 100$  with a deviation from exponential behavior for larger lengths. A characteristic decay length or “screening length”  $\lambda$  is estimated from linear fits to the lin-log data for  $z/a < 100$  (see Fig. 5). As we can see from these plots a nice data collapse is obtained, indicating that the invasion probability density  $\phi(z)$ , and thus the screening length  $\lambda$ , are independent of the capillary number for a given system. On the other hand, when comparing the two systems, the screening length  $\lambda$  depends on the system size:  $\lambda = (54 \pm 10)$  mm for the wide model, and  $\lambda = (34 \pm 5)$  mm for the narrow model. The actual shape of function  $\phi$  also seems to be weakly dependent on the system size.

Relating the mass of the frozen structure,  $n(z)$ , to the invasion probability density,  $\phi(z)$ , and confronting the obtained relation to experimental results, provides new insights into the displacement process. The total number of invaded pores in a time interval  $[t, t + \Delta t]$  is  $R \times \Delta t$ , where  $R$  is the number of invaded pores per time unit.

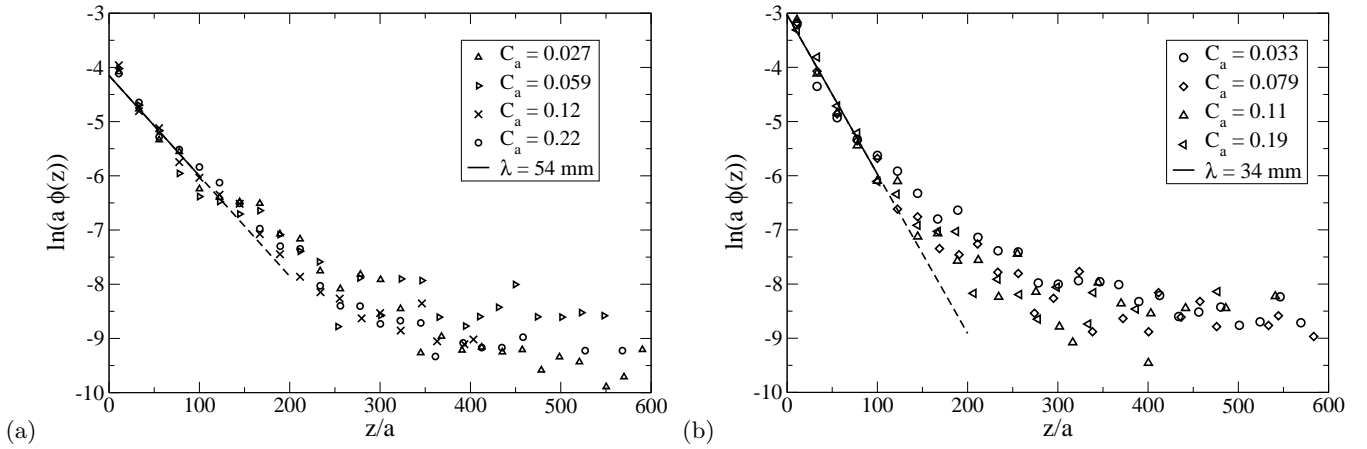


FIG. 5: *Lin-log plot of the invasion probability density  $\phi(z)$  as a function of the distance  $z$  to the finger tip. The indicated distribution corresponds to (a) data from the wide experimental model and (b) from the narrow model. The solid lines in the curves corresponds to the model function  $\ln(Be^{-z/\lambda})$  obtained from linear regression over  $\ln(\phi(z))$  for  $z/a < 100$ .*

For a given flow rate  $Q$ ,  $R$  is related to  $Q$  and to the characteristic pore volume  $V_{\text{pore}}$  by the relation  $Q = R \times V_{\text{pore}}$ , so that

$$R = \frac{W}{a^2} v_f, \quad (2)$$

where  $W$  is the width of the system,  $a$  is the characteristic pore size, and  $v_f$  is the Darcy or filtering velocity of the wetting fluid; for a given porous medium and fluid pair  $v_f \propto C_a$ . The number of invaded pores in the analysis strip defined by  $z \in [z, z + \Delta z]$  during time interval  $[t, t + \Delta t]$  is then  $R \Delta t \times \phi(z) \Delta z$ . The tip position  $z'_{\text{tip}}$  is further given by  $z'_{\text{tip}}(t) = z'_0 + v_{\text{tip}} t$  where  $v_{\text{tip}}$  is the speed of the finger tip (assumed to be constant) and  $z'_0 = z'_{\text{tip}}(t=0)$ . This is a fairly good approximation after a short initial regime as seen in Fig. 4.

The total number of invaded pores in an analysis strip at distance  $z$  from the finger tip and in a strip of width  $\Delta z$  is thus given by:

$$n(z) \Delta z = R \int_{t_0}^t \phi[z(t')] \Delta z dt', \quad (3)$$

where  $t_0$  is the time at which  $z'_{\text{tip}} = z'$ . Taking advantage of the linear relation between the coordinate  $z$  and tip speed  $v_{\text{tip}}$ ,  $z(t) = z'_{\text{tip}}(t) - z'_{\text{tip}}(t_0) = (t - t_0) v_{\text{tip}}$ , Eq. (3) becomes

$$n(z) = \frac{R}{v_{\text{tip}}} \int_0^z \phi(\tilde{z}) d\tilde{z} \equiv \frac{R}{v_{\text{tip}}} \Phi(z). \quad (4)$$

Using Eq. (2) we finally obtain the relation

$$n(z) = \frac{W v_f}{a^2 v_{\text{tip}}} \Phi(z) \propto \frac{C_a}{v_{\text{tip}}} \Phi(z), \quad (5)$$

which relates the linear density of invaded pores (or “cluster-mass” density),  $n(z)$ , to the cumulative invasion probability density distribution,  $\Phi(z)$ . This relation is

confirmed by Fig. 6, where  $n(z) \times (a^2 v_{\text{tip}} / (W v_f))$  is plotted as a function of  $z/a$ . All experimental plots collapse, confirming that there is one single cumulative probability distribution  $\Phi(z)$  for the system for all experiments at different extraction speeds. The function  $\Phi(z)$ , computed as an average function from all cumulative probability functions for the various experiments, is plotted in Fig. 6 as a plain line.

The insert of Fig. 6 shows  $(a^2 v_{\text{tip}}) / (W v_f) (n_\infty - n(z))$  on a lin-log scale, where  $n_\infty \equiv W v_f / a^2 v_{\text{tip}}$ . The solid lines represents  $(1 - \Phi(z))$  and the dashed lines  $(1 - e^{-z/\lambda})$  which would be the model function for a pure exponential  $\phi$  ( $\lambda$  is the screening length evaluated before).

From the results presented above we conclude that the active invasion zone is defined by a screening length  $\lambda$  which is constant for a given porous media and liquid pair and at a range of capillary numbers of two decades. However, we expect this result to be valid only for sufficiently high filtration speed  $v_f$ . Indeed, on the one hand, the capillary fingering regime ( $C_a \simeq 0$ ) corresponds to an invasion that is controlled by fluctuations in the capillary threshold pressures, so that invasion occurs along the whole front [6, 16]. There is no well defined finger tip or growth direction in that limit. The width of the capillary threshold pressure distribution  $W_c$  is larger than the viscous pressure drop over the whole system and defining a screening length or active zone is not meaningful.

When the length of the system is larger than its width, it is found from both pressure measurements and simulations that the decay in pressure into the structure from the longest finger occurs on a length scale of the order of the width of the system (see Fig. 2). We therefore expect  $W$  and not  $L$  to be the relevant length scale for the decay of the pressure field close to the tip. Viscous forces can therefore be considered to dominate capillary pressures if the following criteria is met:

$$W_c < \frac{W \mu v_f}{\kappa}, \quad (6)$$

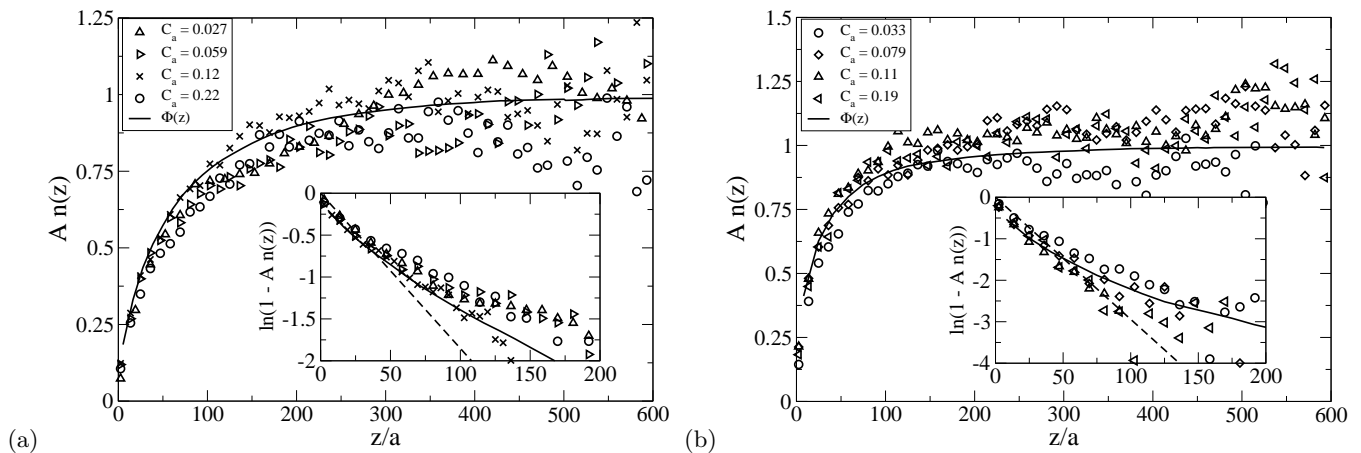


FIG. 6: Plot of the rescaled average mass density of non wetting fluid  $A \times n(z)$  where  $A = a^2 v_{tip}/(W v_f)$  inside the model as a function of the distance to the tip of the most advanced finger  $z$ : (a) the wide model and (b) the narrow model. The average cumulative invasion probability function  $\Phi(z)$  is plotted on top of the curves for comparison in the two cases. The inserts of (a) and (b) show the plots  $\ln[1 - (a^2 v_{tip}/(W v_f)) n(z)] = \ln[(a^2 v_{tip})/(W v_f)] + \ln[(n_\infty - n(z))]$  as a function of  $z$ . The solid lines in the inserts correspond to  $\ln(1 - \Phi(z))$ , and the dashed lines has the slope  $1/\lambda$  where  $\lambda$  is the screening length of  $\phi(z)$  found from Fig. 5, i.e. respectively  $\lambda = (54 \pm 10)$  mm and  $(34 \pm 5)$  for the wide model and narrow model.

or if we assume  $W_c \sim P_c$  (which is the case here)

$$C_a > a/W \quad . \quad (7)$$

For our system  $a/W \sim 10^{-3}$ , which is an order of magnitude smaller than our lowest capillary number.

On the other hand, for situations where the “pure viscous fingering” in a random porous media has been reached, there is no trapping of wetting liquid inside the fingers, which reached the lower one pore width limit (at  $C_a \approx 0.2$  in our system). Whether the screening length or active zone have the same width or behave identically as for lower capillary numbers is not clear. We believe that the screening by the most advanced finger is a viscous effect, which remains important as the displacement speed increases. In this one pore limit however, the tip speed dependence on the capillary number is modified, as will be further detailed in section III B

### 3. The relation between the growth probability density $\phi(z)$ and the fluid pressure.

Fig. 7 shows the dependence of the pressure difference  $\Delta P(z) = P(z) - P(\infty)$  in the wetting liquid as a function of the distance  $z$  to the outermost tip for different capillary numbers. Here  $P(\infty) \equiv P_0 - P_c(\infty)$  is the liquid pressure along the interface far behind the finger tip, with  $P_0$  the pressure in the non-wetting liquid and  $P_c(\infty)$  the capillary pressure in this stagnant zone. It is important to note that the pressure  $P(z)$  is measured on the side of the model (indicated in Fig. 2) while the fingers are propagating in the central part of the model (Fig. 2).

The pressure seems to be linearly dependent on the distance from the tip during a first stage before the tip

reaches the sensor. In a second stage, after the finger tip has passed the sensor, pressure relaxes and reaches the value  $P(\infty)$ . A closer inspection of the pressure curves (see Fig. 7) shows that there is no clear systematic dependence of the pressure relaxation on the capillary number. The pressure difference  $P(z) - P(\infty)$  decays with approximately the same length for the different capillary numbers (see insert of Fig 7). This indicates that the details of the internal structure of the “fingers” do not have a strong influence on the pressure field on large scales.

The pressure measurements are related to the invasion activity by the following considerations. Let us consider the local speed of an interface located in an arbitrary pore throat between two pores, one filled with air and the other with the wetting-liquid. Let  $P(x, z)$  be the pressure in the wetting liquid and  $P_t(x, z)$  be the capillary pressure threshold value to invade that pore. Note that this is different from the pressure  $P(z)$  defined as the pressure measured on the side of the model at the sensor position. The pore throat at position  $(x, z)$  is passed under the condition that the capillary pressure  $P_c(x, z) = P_0 - P(x, z)$  is larger than the capillary threshold pressure  $P_t(x, z)$  at this position. If invasion occurs, a characteristic value of the speed of the interface will be:

$$v(x, z) = \frac{2\kappa}{\mu} \frac{(P_0 - P(x, z) - P_t(x, z))}{a} \quad . \quad (8)$$

Let  $N(P_t(x, z))$  be the capillary pressure distribution. For the sake of simplicity, we assume a flat capillary pressure distribution with lower limit  $P_t^{\min}$ , upper limit  $P_t^{\max}$  and width  $W_c$ . Then, the expectational value of the interface velocity (average value over the capillary threshold distribution), while the pore is getting invaded will be

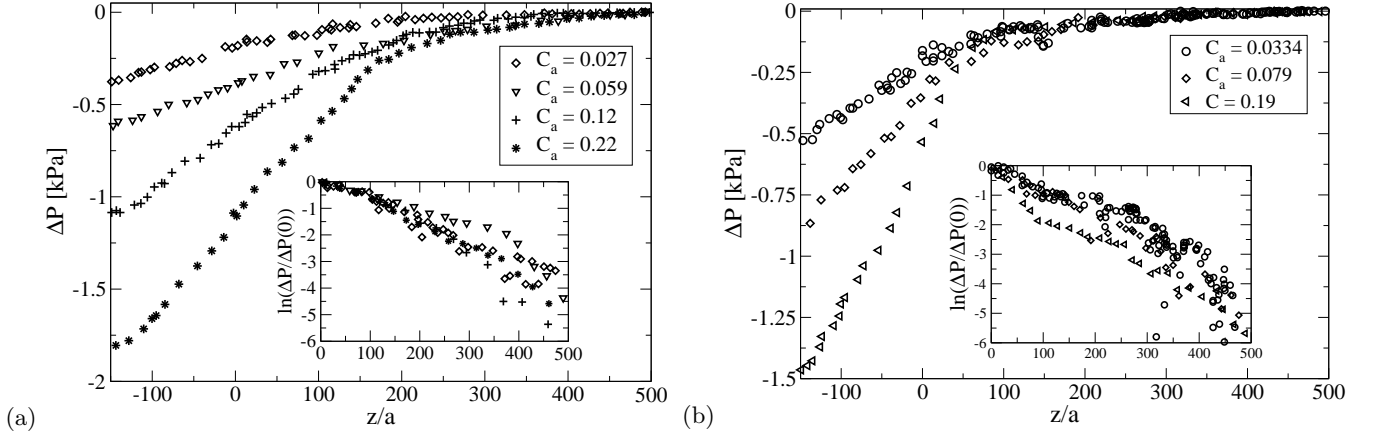


FIG. 7: Plot of the pressure difference  $\Delta P(z) = P(z) - P(\infty)$  measured by the pressure sensor located in the position  $(x_s, z'_s) = (38 \text{ mm}, 280 \text{ mm})$ . The insert is the same data plotted in a semi-log plot where  $\Delta P(z)$  is scaled with  $\Delta P(0) = P(z=0) - P(\infty)$  to illustrate the decay of the pressure field. Figure (a) is for the wide model and Figure (b) is for the narrow model.

$$\langle v(x, z) \rangle = \frac{1}{P_0 - P(x, z) - P_t^{\min}} \int_{P_t^{\min}}^{P_0 - P(x, z)} \frac{2\kappa}{a\mu} (P_0 - P(x, z) - P_t(x, z)) dP_t = \frac{\kappa}{a\mu} (P_0 - P(x, z) - P_t^{\min}) \quad . \quad (9)$$

Here,  $P_t^{\min}$  is the minimum of the distribution for capillary threshold; when  $P_0 - P(x, z)$  goes to that minimum, the expectational value for the speed of the interface goes to zero. The growth probability density  $\phi(x, z)$  for the invasion structure within a time  $[t, t + \Delta t]$  at a position  $(x, z)$  is proportional to  $\langle v(x, z) \rangle$  times the probability  $p(x, z)$  that the throat gets invaded; hence

$$\phi(x, z) = C \langle v(x, z) \rangle p(x, z) \quad , \quad (10)$$

where  $C$  is a normalization constant, which we can find by integrating the above equation along the invasion front  $S$ :

$$\int_S \phi(x, z) dl = C \int_S \langle v(x, z) \rangle p(x, z) dl \quad (11)$$

$$1 = \frac{C}{a} \int_S a \langle v(x, z) \rangle p(x, z) dl = \frac{C}{a} Q \quad , \quad (12)$$

where  $Q$  is the flow rate, thus:

$$C = \frac{a}{Q} \quad (13)$$

Since we have assumed a flat capillary threshold distribution of width  $W_c$ , the probability that the pore at position  $(x, z)$  gets invaded is

$$p(x, y) = \frac{1}{W_c} (P_0 - P(x, z) - P_t^{\min}) \quad . \quad (14)$$

From Eq. (9 - 14) we obtain for the growth probability density  $\phi(x, z)$  in position  $(x, z)$ :

$$\phi(x, z) = \frac{\kappa}{Q\mu W_c} (P_0 - P_t^{\min} - P(x, z))^2 \quad . \quad (15)$$

Averaging this expression over  $x$  and introducing the number of interface sites at a distance  $z$  from the tip,  $f(z)$ , we obtain the invasion probability density  $\phi(z)$  as

$$\phi(z) = f(z) \langle \phi(x, z) \rangle_x \quad (16)$$

$$\phi(z) = f(z) \frac{\kappa}{Q\mu W_c} (P_0 - P_t^{\min} - \langle P(x, z) \rangle_x)^2 \quad , \quad (17)$$

for which we have assumed that  $P(x, z)$  is a function of  $z$  only (lowest order approximation). Eq. (17) yields

$$\langle P(x, z) \rangle_x = P_0 - P_t^{\min} - \left( \frac{\phi(z)}{f(z)} \frac{QW_c\mu}{\kappa} \right)^{\frac{1}{2}} \quad , \quad (18)$$

which can be rewritten by introducing the relation between the flow rate and the capillary number. Accordingly the average pressure in the wetting fluid in the immediate vicinity of the interface and at position  $z$  is related to the activity  $\phi(z)$  according to

$$\langle P(x, z) \rangle_x = P_0 - P_t^{\min} - \left( C_a \gamma W_c \frac{W}{a} \frac{\phi(z)}{f(z)} \right)^{\frac{1}{2}} \quad . \quad (19)$$

Let us now look closer at the “snapshots” of the experiments shown in Fig. 2. For  $z = 0$ , the last correction term in Eq. (19) is 170 Pa for the fastest experiments ( $C_a = 0.22$ ), and 65 Pa for the slowest experiments ( $C_a = 0.027$ ). At the same moment, the imposed external pressures in the outlet channel are 3055 Pa for the fastest and 625 Pa for the slowest experiments. The minimum capillary pressure is estimated to 373 Pa, and the width of the capillary distribution to 200 Pa. This

indicates that the correction term in Eq. (19) should not be neglected. In Fig. 2 is shown the gray scale map of the pressure field at a particular time, simulated from the displacement structures obtained experimentally. A very strong screening is seen for all injection rates. The large scale structure of the pressure field in the vicinity of tip of the longest finger looks visually very similar even if the invader structure is quite different. In the simulations of the pressure field we have used Eq. (19) to set the proper boundary conditions. The pressure field has been calculated by solving the Laplace equation for the pressure using a conjugate gradient method [23]. We used the boundary condition given by Eq. (19) on the cluster and the inlet line. As boundary condition on the outlet we used the pressure  $P(\infty) - \Delta P_{\text{tot}}$ , where  $-\Delta P_{\text{tot}}$  is the total viscous pressure drop imposed in the corresponding experiment at that moment. To obtain  $P(\infty) = P_0 - P_c(\infty)$ , the capillary pressure  $P_c(\infty)$  was measured in the experiments for large values of  $z$ . Fig. 8 shows the simulated pressure  $\Delta P(x_s, z) = P(x_s, z) - P(\infty)$  as a function of the  $z$ -coordinate relative to the tip position defined as previously, at a fixed lateral position  $x_s$  corresponding to the  $x$ -coordinate of the pressure sensor. It is important to note that this is somewhat different from the experiments since the pressure is measured at different  $z'$  positions, but at the same time, i.e. with a fixed geometry of the invasion cluster, while in the experiments the pressure is measured at a fixed  $z'$  position, at different times corresponding to various stages of the invasion cluster. The length scale of the decay of the pressure for  $z > 0$  is very similar in the experiments and the simulations (see comment below). However the pressure difference  $\Delta P(z)$  in the simulations is lower than the  $\Delta P(z)$  measured by the sensor (at position  $(x_s, z'_s) = (38 \text{ mm}, 280 \text{ mm})$ ) in the model (see Fig. 7). This is due to the strong boundary effects of the pressure close to the outlet channel: the tips in the simulations situations are very close to this boundary along which the pressure is fixed (see Fig. 2), while in the situations corresponding to the measurements at  $z < 0$  plotted in Fig. 7, the outlet boundary was far ahead of the finger tip, and the pressure boundary condition was equivalent to an imposed gradient at infinite distance. To check the importance of this boundary effect on the magnitude of the pressure difference, the simulated pressure has been compared with the pressure difference  $\Delta P(z)$  evaluated from measurements at the outlet channel, as the finger tip progressed further than the stage corresponding to the simulations. The agreement in Fig. 8 between the simulated pressure and the data points corresponding to the outlet channel measurements is then satisfactory.

To compare the length scale of the decay of the pressure for  $z > 0$  between the simulations and the experiment, we then compare the pressure data measured inside the model at sensor position, to the simulation data scaled by a factor such as  $\Delta P(x_s, z = 0)$  would be equal in experiments and simulations. Such rescaling of the

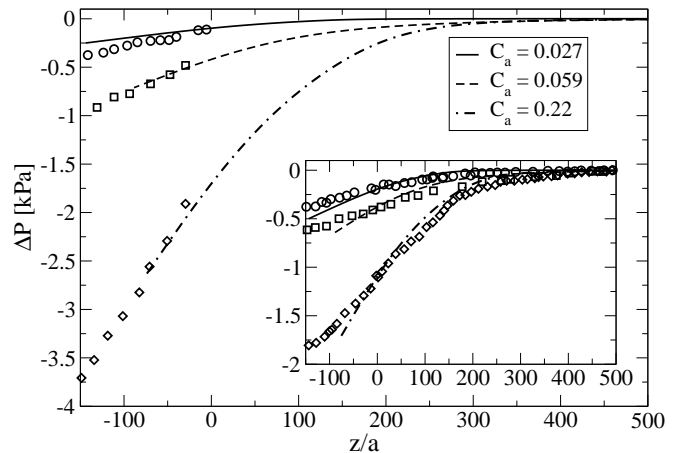


FIG. 8: The simulated pressure along the line with  $x_s = 38 \text{ mm}$  (corresponding to the  $x$  coordinate of the pressure sensor) for the invasion structures in Fig. 2. The data points in the main graph show the corresponding pressures measured at the outlet sensor. In the insert we plot scaled simulation data with corresponding pressure data measured inside the model at  $(x_s, z'_s) = (38 \text{ mm}, 280 \text{ mm})$ .

simulation pressure profile simply corresponds to the result of an identical simulation still carried on the invasion clusters of Fig. 2, with identical boundary conditions derived from the growth density function for the pressure along the clusters, but where the imposed pressure along the bottom boundary is such that the pressure at point  $(x_s, z'_{tip})$  would coincide with the pressure measured in the experiments when the tip passed at the same height as the sensor, i.e. when  $z'_{tip} = z'_s$ . This ensures that the pressure gradient and pressure value in the region around the tip of the invading cluster are of the same order in these rescaled simulations and in the experimental stages corresponding to  $z \sim 0$  in Fig. 7, which is a first order technique to correct for the strong boundary effect and compare with these experimental situations where the bottom boundary is much further away. The pressure measured in the experiments at sensor position and this scaled simulation data are plotted in the insert of Fig. 8. This comparison shows that the decay in the pressure happens at comparable length scales in the simulations and experiments.

Eventually, the local structure of the finger and the lateral  $x$ -distance from the invader to the pressure sensor will also have an important influence on the pressure field. The difference in the pressure field between the left and the right side of the finger (looking in the flow direction) in Fig. 2 illustrates this point. The deviation between the experimental data points and the simulations for the lowest capillary number of the main part of Fig. 8 may be explained by this effect. As the lateral position  $x_{tip}$  of the invading structure moves during the experiment, and is importantly varying from an experiment to the next, this effect also explains the important dispersion of the scaled pressure drops  $\Delta P(z)/\Delta P(0)$  observed



in the insert of Fig. 7 (b).

### B. Capillary number dependent features

As stated in the introduction to section III, Fig. 2 clearly shows that some features of the invading cluster depend on the capillary number. The mass  $n(z)$  of the invasion cluster obviously decreases with increasing capillary number; in relation to this, the speed of the most advanced finger tip,  $v_{\text{tip}}$ , increases with the capillary number, and there is a systematic trend for fingers to become thinner as capillary number increases. In the following we first present results relative to the “mass density” in the stagnant zone,  $n_\infty$ , and to the velocity of the most advanced fingertip,  $v_{\text{tip}}$ . In the end we discuss the results relative to measurements of the characteristic width of the finger-like structures, the definition of which are not as straightforward and clear as those of  $n_\infty$  and  $v_{\text{tip}}$ .

The evolution of the average mass density in the stagnant zone  $n_\infty$  as a function of the capillary number is presented in Fig. 9 (a) on a log-log scale. The data is consistent with a scaling law in the form  $n_\infty \propto C_a^{-\alpha}$ , with a scaling exponent  $\alpha = 0.65 \pm 0.05$  for both the wide and narrow models. Here  $n_\infty$  has been measured by fitting the function  $n_\infty [1 - \exp(-z/\lambda)]$  with both parameters free to our measured  $n(z)$  data. Due to that dependence of the mass of the invasion cluster on the capillary number (Fig. 9 (a)), the speed of the most advanced finger tip,  $v_{\text{tip}}$ , is expected to depend on the filtration speed or capillary number in a non-linear way. The saturated mass density and the speed of the most advanced finger are related to each other through Eq. 5, according to

$$v_{\text{tip}} \propto \frac{C_a}{n_\infty} . \quad (20)$$

Based on that argument,  $C_a/v_{\text{tip}}$  should therefore scale in the same way as  $n_\infty$  with respect to the capillary number. In Fig. 9 (b), the quantity  $C_a/v_{\text{tip}}$  is plotted as a function of  $C_a$  using a log-log scale. The plot is consistent with the expected scaling (20) and the result for the mass density presented above.

The study of the dependency of the finger width on the capillary number is somewhat less straightforward, because our invading clusters structures exhibit extensive branching and display “fingers” both at small scales as “capillary fingers” and at large scales as “viscous fingers”. Thus, a precise definition of a finger, and furthermore a finger width, is not an easy task for those structures. A possible method to determine the viscous finger width would consist in finding the characteristic crossover length between geometric features characteristic of viscous fingering and those characteristic of capillary fingering from the density-density correlation function of the structures. However, due to the small difference in fractal dimension between the two regimes,  $1.83 \pm 0.01$  [6, 16]

for capillary fingering and  $1.62 \pm 0.04$  [21, 24] for viscous fingering, larger systems would be necessary for this method to be accurate enough. An experimental determination of the characteristic width  $w_f$  for viscous fingers was previously obtained for *imbibition* experiments [17], for which the characteristic finger width can be defined and found in a more straightforward manner. The obtained scaling was  $w_f \propto C_a^{-0.5}$ . In those imbibition experiments, the finger width  $w_f$  was measured as the average length of cut-segments perpendicular to the flow direction. This method can also be applied in our experiments, but due to the small scale fractal nature of the invasion front, trapping of wetting fluid inside the fingers and capillary fingering on small length scales, it is not obvious which length scales are being probed with this method. The results that we obtain are plotted as a function of the capillary number in Fig. 10. Clusters of wetting liquid trapped behind the displacement front have been removed from the picture prior to analysis. We then define the front width  $w_f$  as the average over  $z$  and time of the length of the intersects between the invasion cluster emptied from these trapped regions and cuts perpendicular to the flow direction.

The measurements are consistent with a scaling law in the form  $w_f \propto C_a^{-\beta}$ , with  $\beta = 0.75 \pm 0.05$ . This is significantly different from what was measured for imbibition. It also differs significantly from the scaling law expected from theoretical arguments for percolation in a destabilizing gradient [25, 26] for two-dimensional systems:  $w_f \propto C_a^{-\beta}$  with  $\beta = 0.57$ . In our experiments, the destabilizing field (pressure) is highly inhomogeneous, which may explain why the behavior expected from the percolation in a gradient theory is not really observed.

From Fig. 9 and 10, the observed scalings appear to be valid for a limited range of capillary numbers. For high capillary numbers the observed scaling breaks down for  $C_a \approx 0.2$ , which corresponds to situations where the characteristic finger width have reached the one pore limit. At the other limit, for small capillary numbers we don’t seem to reach the lower limit in capillary number. But we expect that the observed scaling brake down for capillary numbers smaller than the criteria given in Eq. (7),  $C_a \sim 10^{-3}$ .

## IV. CONCLUSION AND PROSPECTS

We have studied the dynamics of the invasion process observed during drainage in a two-dimensional porous medium, for extraction speeds that result in an unstable fingering of the displacing non-wetting fluid into the displaced wetting fluid.

Our main finding is that for a given porous medium, the displacement is controlled by an invasion probability density that only depends on the distance of the point where it is measured to the tip of the most advanced finger tip, and is independent of the capillary number. The decay of this invasion probability density,  $\phi(z)$ , de-

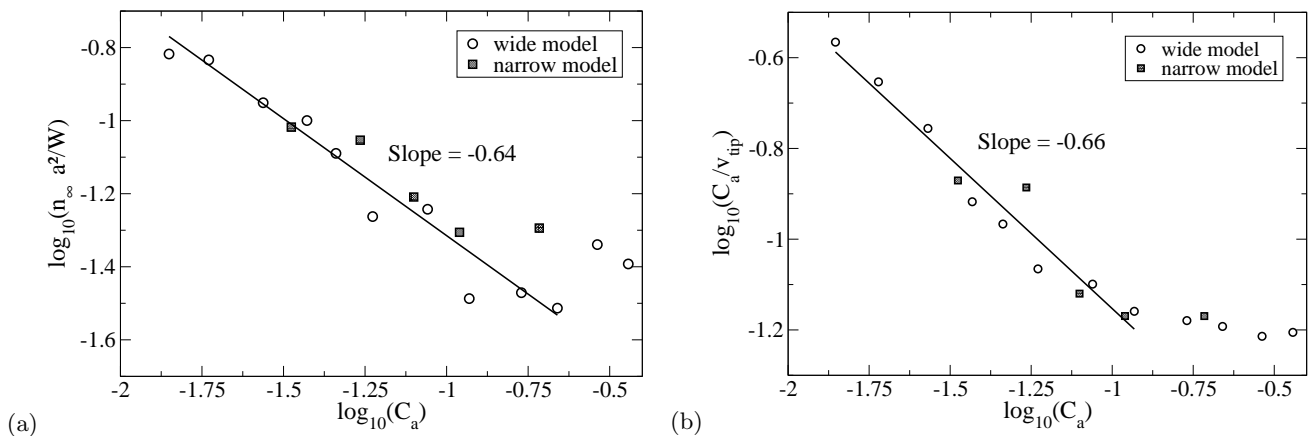


FIG. 9: Log-log plots of (a) the saturated mass density,  $n_{\infty}$ , and (b) of the speed of the most advanced finger,  $v_{tip}$ , as a function of the capillary number, for the two set of experiments. Both plots are consistent with a scaling in the form  $n_{\infty} \propto C_a/v_{tip} \propto C_a^{-\alpha}$ , with  $\alpha = 0.65 \pm 0.05$ .

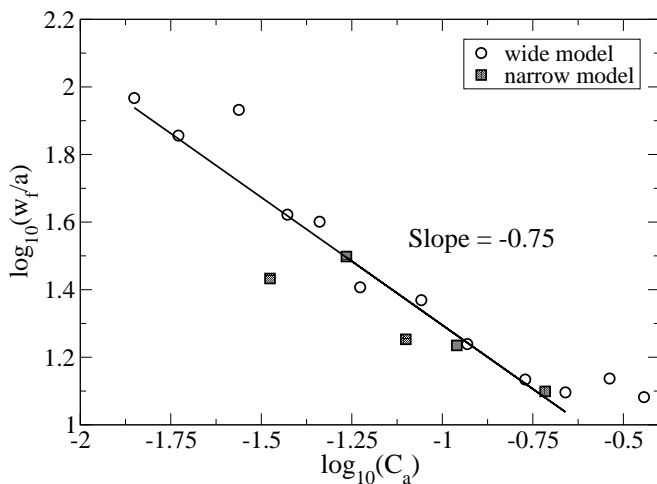


FIG. 10: Log-log plot of the measured characteristic width of the finger like structures as a function of the capillary number, for both the wide and narrow model. The data is consistent with a scaling of the finger width in the form  $w_f \propto C_a^{-\beta}$ , with  $\beta = 0.75 \pm 0.05$ .

defines an active zone for the invasion process, outside of which the viscous pressure field can be considered to be screened by the invasion structure. In particular, parts of the invasion structure lying outside this active zone are frozen and do not evolve in time any more. The size of the active zone, of characteristic screening length,  $\lambda$ , was found to be independent of the capillary number for a wide range of injection rates. In addition, exper-

iments carried out on models with two different widths suggested that the invasion probability density appears to be capillary number independent, its actual shape being possibly fixed by the system size. While the invasion process is described by an invasion probability density that is independent of the capillary number, the invasion speed and displaced volume in the stagnant zone were found to scale on the capillary according to power laws,  $n_{\infty} \propto C_a/v_{tip} \propto C_a^{-0.65}$ .

The link between the growth probability and the pressure field has been studied. An expression for the pressure boundary condition on the cluster has been calculated which relates the pressure on the interface of the invader to the growth probability density function  $\phi(z)$ . The measured pressure has been compared to the corresponding simulated pressure by solving the Laplace equation for the pressure field using this expression for the boundary condition on the cluster. A good agreement is found between the simulations and the experiments.

System size dependencies should be subject to further investigations, both experimentally and by means of computer simulations.

## V. ACKNOWLEDGMENTS

The work was supported by NFR, the Norwegian Research Council, VISTA, the Norwegian academy of science and letters' research program with Statoil and the French/Norwegian collaboration PICS.

- 
- [1] J. Bear, *Dynamics of Fluids in Porous Media* (American Elsevier Publishing Company, New York, 1972).  
 [2] F. A. L. Dullien, *Porous Media Fluid Transport and Pore Structure* (Academic Press, Inc., San Diego, 1992), 2nd

- ed.  
 [3] M. Sahimi, *Rev. Mod. Phys.* **65**, 1393 (1993).  
 [4] M. Sahimi, *Flow and Transport in Porous Media and Fractured Rock* (VCH Verlagsgesellschaft mbH, Wein-

- heim, Germany, 1995).
- [5] R. Lenormand, E. Touboul, and C. Zarcone, *Journal of Fluid Mechanics* **189**, 165 (1988).
  - [6] R. Lenormand and C. Zarcone, *Transport in Porous Media* **4**, 599 (1989).
  - [7] P. G. Saffman and G. Taylor, *Proc. Soc. London Ser. A* **245**, 312 (1958).
  - [8] T. A. Witten and L. M. Sander, *Physical Review Letters* **47**, 1400 (1981).
  - [9] M. Plischke and Z. Racz, *Phys. Rev. Lett.* **53**, 415 (1984).
  - [10] M. Plischke and Z. Racz, *Phys. Rev. Lett.* **54**, 2054 (1985).
  - [11] P. Meakin, A. Coniglio, H. E. Stanley, and T. A. Witten, *Phys. Rev. A* **34**, 3325 (1986).
  - [12] T. C. Halsey, P. Meakin, and I. Procaccia, *Physical Review Letters* **56**, 854 (1986).
  - [13] C. Amitrano, A. Coniglio, and F. di Liberto, *Physical Review Letters* **57**, 1016 (1986).
  - [14] B. B. Mandelbrot, *Journal of Fluid Mechanics* **62**, 331 (1974).
  - [15] L. Paterson, *Phys. Rev. Lett.* **52**, 1621 (1984).
  - [16] R. Lenormand and C. Zarcone, *Physical Review Letters* **54**, 2226 (1985).
  - [17] J. P. Stokes, D. A. Weitz, J. P. Gollub, A. Dougherty, M. O. Robbins, P. M. Chaikin, and H. M. Lindsay, *Physical Review Letters* **57**, 1718 (1986).
  - [18] D. A. Weitz, J. P. Stokes, R. C. Ball, and A. P. Kushnick, *Physical Review Letters* **59**, 2967 (1987).
  - [19] R. Lenormand, C. Zarcone, and A. Sarr, *Journal of Fluid Mechanics* **135**, 337 (1983).
  - [20] R. Lenormand, *J. Phys.: Condens. Matter* **2**, SA79 (1990).
  - [21] K. J. Maloy, J. Feder, and T. Jossang, *Physical Review Letters* **55**, 2688 (1985).
  - [22] Y. Meheust, G. Lovoll, K. J. Maloy, and J. Schmittbuhl, *Physical Review E* **66**, 51603 (2002).
  - [23] G. G. Batrouni and A. Hansen, *J. Stat. Phys.* **52**, 747 (1988).
  - [24] J.-D. Chen and D. Wilkinson, *Physical Review Letters* **55**, 1892 (1985).
  - [25] R. Lenormand, *Proc. R. Soc. Lond. A* **423**, 159 (1989).
  - [26] Y. C. Yortsos, B. Xu, and D. Salin, *Computational Geosciences* **5**, 257 (2001).